Geophysical Research Letters

RESEARCH LETTER
10.1029/2019GL084715

Nanogoethite as a Potential Indicator of Remagnetization in Red Beds

Wentao Huang[1,2], Michael J. Jackson[3], Mark J. Dekkers[4], Peat Solheid[3], Bo Zhang[5], Zhaojie Guo[5], and Lin Ding[1]

[1]Key Laboratory of Continental Collision and Plateau Uplift, Institute of Tibetan Plateau Research, and Center for Excellence in Tibetan Plateau Earth Sciences, Chinese Academy of Sciences, Beijing, China, [2]Department of Earth and Environmental Sciences, University of Rochester, Rochester, NY, USA, [3]Institute for Rock Magnetism, Department of Earth Sciences, University of Minnesota, MN, USA, [4]Department of Earth Sciences, Utrecht University, Utrecht, The Netherlands, [5]Key Laboratory of Orogenic Belts and Crustal Evolution, Ministry of Education, School of Earth and Space Sciences, Peking University, Beijing, China

Abstract Red beds are well-known for recording stable natural remanent magnetization (NRM). However, discriminating primary NRM from secondary remanence in red beds is difficult. The Paleogene Nangqian red beds in eastern Tibetan Plateau variably record an overprint related to nearby magmatism and thus provide a great opportunity to characterize remagnetization in red beds. Through comprehensive rock magnetic, Mössbauer spectroscopic, and petrographic analyses, we find that remagnetization was controlled by temperature. Remagnetized red beds contain abundant authigenic hematite and goethite, with some larger grains unblocking at the Néel temperatures and the remainder (nanoparticles) unblocking at lower temperatures. In contrast, red beds retaining primary NRM are characterized by dominance of detrital hematite and magnetite, presence of fine-grained authigenic hematite, and absence of authigenic goethite and magnetite. High temperature behaviors of NRM/susceptibility are indicative of remagnetization, but the presence of goethite appears to be a more sensitive criterion for diagnosing remagnetization in red beds.

Key Points:
- Remagnetization of the Paleogene Nangqian red beds in eastern Tiebtan Plateau was controlled by temperature
- Remagnetization was induced by replacing of detrital magnetite and hematite by authigenic magnetite and hematite
- The presence of abundant nanogoethite appears to be a sensitive criterion for diagnosing remagnetization in red beds

Supporting Information:
- Supporting Information S1

Correspondence to:
W. Huang,
whuang28@ur.rochester.edu

Citation:
Huang, W., Jackson, M. J., Dekkers, M. J., Solheid, P., Zhang, B., Guo, Z., & Ding, L. (2019). Nanogoethite as a Potential Indicator of Remagnetization in Red Beds. *Geophysical Research Letters*, *46*, 12,841–12,850. https://doi.org/10.1029/2019GL084715

Received 25 JUL 2019
Accepted 21 OCT 2019
Accepted article online 15 NOV 2019
Published online 20 NOV 2019

The copyright line for this article was changed on 23 NOV 2019 after original online publication.

1. Introduction

Red beds, siliciclastic rocks pigmented by hematite, have been extensively investigated for paleogeography and magnetostratigraphy (e.g., Dupont-Nivet et al., 2007; Xian et al., 2019). The prevailing hypothesis states that large detrital hematite grains in red beds carry a primary depositional remanent magnetization (DRM) (e.g., Kruiver et al., 2000), whereas the fine-grained pigmentary hematite carries a secondary chemical remanent magnetization (CRM). The CRM, possibly formed long after deposition of the red beds, can partially or completely obscure the DRM well below the Néel temperature of hematite and complicates paleomagnetic interpretations (e.g., Deng et al., 2007; Stearns & Van der Voo, 1987). A central aspect of paleomagnetic studies on red beds is thus to distinguish CRM from DRM, which is, however, difficult because the mechanism of CRM acquisition and the characteristics of authigenic hematite are not well understood. While experimental study shows that CRM has wide spectrum of unblocking temperature (200–650 °C) in contrast to that of the DRM (600–680 °C) (Jiang et al., 2015), paleomagnetic studies of natural samples reveal that thermal unblocking spectra of CRM can overlap with that of the DRM and extend up to the Néel temperature (Jiang et al., 2017; Swanson-Hysell et al., 2019). Uncertainty thus exists in interpreting the origin of the remanence carried by high-unblocking-temperature hematite in red beds, whereas traditional paleomagnetic field tests, even when available, often provide only weak constraints on the timing of remanence acquisition. Therefore, rigorous criteria independent from paleomagnetic directional information are required for evaluating the origin of the remanence isolated at the highest unblocking temperatures and diagnosing insidious remagnetization in red beds.

The Cenozoic Nangqian basin, located in the eastern Qiangtang terrane of the Tibetan Plateau (Figure 1a), was formed by flexural subsidence of the lithosphere in the footwall of a thrust fault activated soon after India-Asia collision (Horton et al., 2002). It is filled with alluvial conglomerate and fluvial sandstone in the older southern part of the basin and deltaic and lacustrine interbedded limestone, gypsum, and reddish mudstone and siltstone in the younger northern part (Li et al., 2018). Age constraints of the basin are based

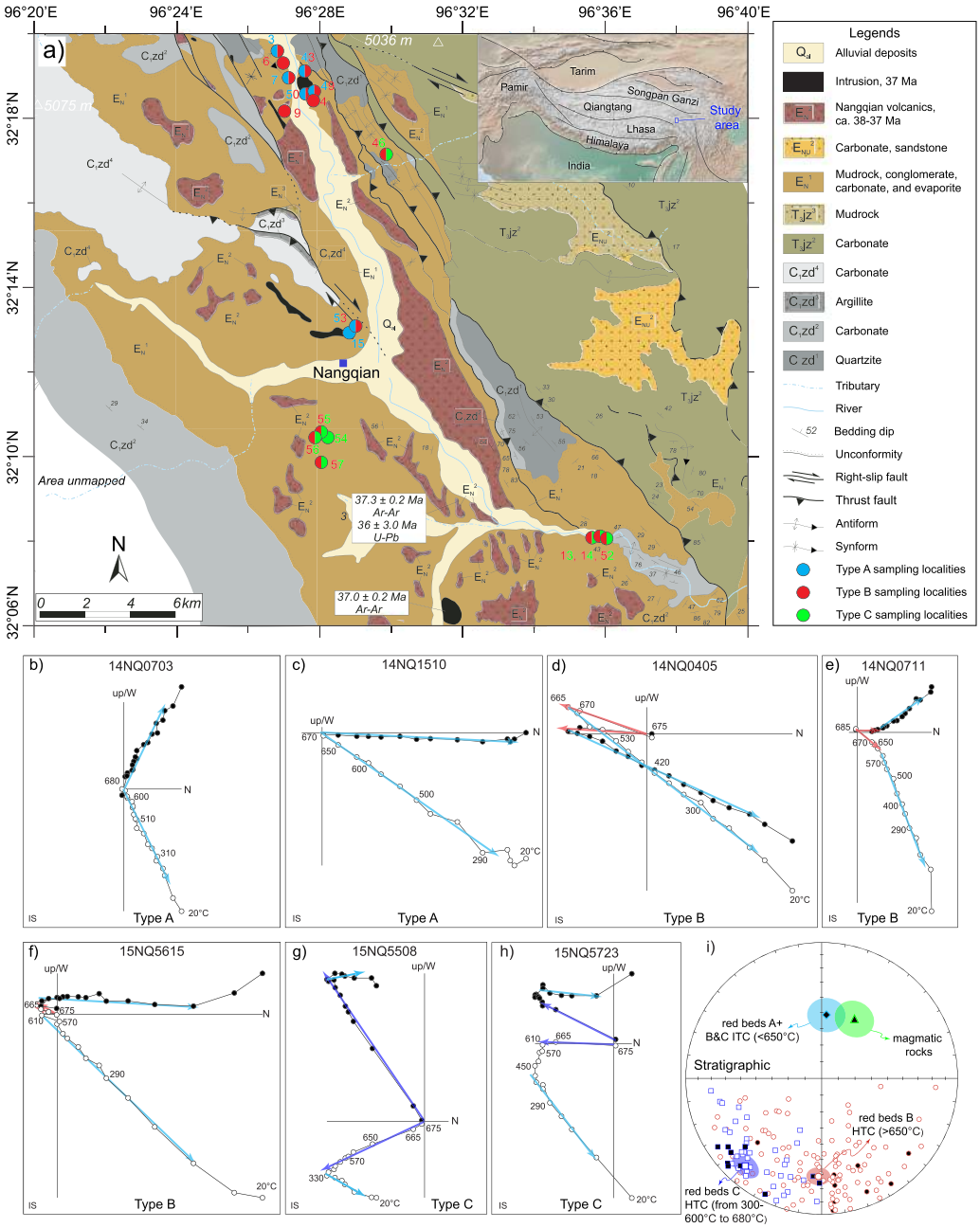

Figure 1. Previous paleomagnetic work in the Cenozoic Nangqian basin. (a) Geologic map of the Nangqian basin (Spurlin et al., 2005) with plotted paleomagnetic sampling localities of red beds, numbers represent site names (14NQXX or 15NQXX). Each site includes 11–24 individual cores (Roperch et al., 2017). (b–h) Thermal demagnetization trajectories of representative samples from the Nangqian red beds with three types (A, B, and C) identified. IS—in situ, circles—inclination, dots—declination. (i) Equal-area projections of the remanent magnetization isolated at high temperatures from individual Type B (red circles) and Type C (blue square) samples in stratigraphic coordinates. Average of the site-mean directions of the primary remanence carried by magmatic rocks (green triangle) and of the overprint recorded by red beds (blue diamond) are also plotted. Shaded circles are the 95% confidence interval.

on Paleogene fossils in the sedimentary rocks, and intrusions and volcanic rocks interbedded with the uppermost strata at 38–37 Ma (Spurlin et al., 2005).

Prior paleomagnetic investigations of the Nangqian basin (Figure 1a) indicate that the red beds carry an overprint with a different direction from that of the present day dipole field, but with the same direction as that of the primary NRM from the magmatic rocks, suggesting that remagnetization of the red beds is related to magmatism at 38–37 Ma (Roperch et al., 2017). Through careful inspection of the thermal

demagnetization trajectories of Nangqian red beds studied by Roperch et al. (2017), we identify three types of samples: (1) Type A (23% of the total 210 individual samples) has linear decay in remanence and a single magnetic component isolated up to the Néel temperature of hematite (Figures 1b and 1c; supporting information Figures S1a–S1h); (2) Type B (53%) has an intermediate temperature component (ITC) isolated from 200 °C to 650–665 °C, followed by a weak (as low as 3% of the NRM in intensity) high temperature component (HTC) with a different direction and/or polarity isolated up to 680 °C (Figures 1d–1f; Figure S2); (3) Type C (24%) also has two components, but the ITC is usually isolated below 300–600 °C, whereas the HTC is isolated from 300–600 °C to 680 °C (Figures 1g and 1h; Figures S1i–S1t). The remanence of Type A samples and the ITC from Types B and C samples define a site-mean direction indistinguishable from that of the magmatic rocks (Figure 1i). The HTC of individual Type B samples are scattered with a mean direction of declination/inclination = 181.9°/−28.6° ($n = 111$, $k = 5.7$, $\alpha_{95} = 6.2$) after bedding correction, whereas the HTC of individual Type C samples has an elongated distribution and defines a different mean direction of declination/inclination = 221.1°/−15.4° ($n = 46$, $k = 9.1$, $\alpha_{95} = 7.4$) (Figure 1i). Compared to the primary NRM isolated from the coeval red beds in the nearby Gongjue basin (150 km southeast of Nangqian) of the eastern Qiangtang terrane (Tong et al., 2017; Zhang et al., 2018), the mean direction of the HTC of Type B samples has abnormal lower declination and higher inclination, whereas the HTC of Type C samples has similar declination and slightly lower inclination. Considering the Cenozoic regional clockwise rotation history of the eastern Qiangtang terrane, and the possibility that the finer-grained Nangqian red beds may have suffered more from compaction-induced inclination shallowing (Li et al., 2017; Tauxe & Kent, 2004), the HTC of Type C samples probably represents the DRM (biased by inclination shallowing), whereas the HTC of Type B samples was at least contaminated by CRM if not completely overprinted, as in the Type A samples.

The acquisition of CRM with variable unblocking temperatures and clear age constraint in the Nangqian red beds thus provide an ideal natural laboratory to examine the mechanisms of remagnetization in red beds along with pertinent features of remagnetized red beds (Types A and B samples), which can be contrasted to those retaining primary NRM (Type C samples). In this study, we apply comprehensive rock magnetic experiments, Mössbauer spectroscopy analyses, and scanning electron microscopy examinations with associated energy-dispersive X-ray spectrometry analyses, to samples from the Nangqian red beds studied by Roperch et al. (2017), aiming at characterizing the distinct properties of remagnetized red beds. These properties may provide robust property-based criteria for diagnosing remagnetization in red beds in future studies.

2. Results

We first applied a series of rock magnetic tests to understand the magnetic mineralogy and grain size of the Nangqian red beds (Text SI). Room temperature hysteresis loops of the red beds samples are mostly rectangular and show high coercivity (B_c) and remanent coercivity (B_{cr}) values (Figures S3 and S4a, Table S1), consistent with the dominance of hematite as a magnetic carrier. Hysteresis loops of some Type C samples are goosenecked (Figure S3f), indicating a significant contribution from magnetite in addition to the principal magnetic phase of hematite (Tauxe et al., 1996). One baked sample adjacent to the dike has potbellied loops and low saturation remanence ratios ($M_{rs}/M_r = 0.47$). In the plots of M_{rs}/M_s versus B_c, Types A and B samples cannot be discriminated from Type C samples (Figure S4a). The coercivity spectra of all the samples can be fitted by two statistically significant components (Figure S3, Table S2). One component has low coercivity (<130 mT) and contribution (<17%), representing magnetite and/or fine-grained hematite (Özdemir & Dunlop, 2014). The other has high coercivity (>400 mT) and contribution (>83%) and is interpreted to be hematite and/or other hard magnetic carriers. High-temperature magnetic susceptibility versus temperature (κ-T) curves of Types A and B samples show distinct behaviors from Type C samples (Figure 2). Types A and B samples are characterized by quasi-linear and reversible descending trends of the magnetic susceptibility up to 550 °C with most susceptibility lost, followed by a hump and then sharp drop of magnetic susceptibility at >620 °C. In contrast, the hump is reached at 300 °C after quasi-linear and reversible decrease of magnetic susceptibility in Type C samples, and the majority of susceptibility is lost in the sharp drop above 620 °C.

Low temperature AC susceptibility measurement of a Type B sample reveal a dependence of susceptibility on both temperature and frequency, persisting at 300–20 K (Figure S5), suggesting a broad blocking

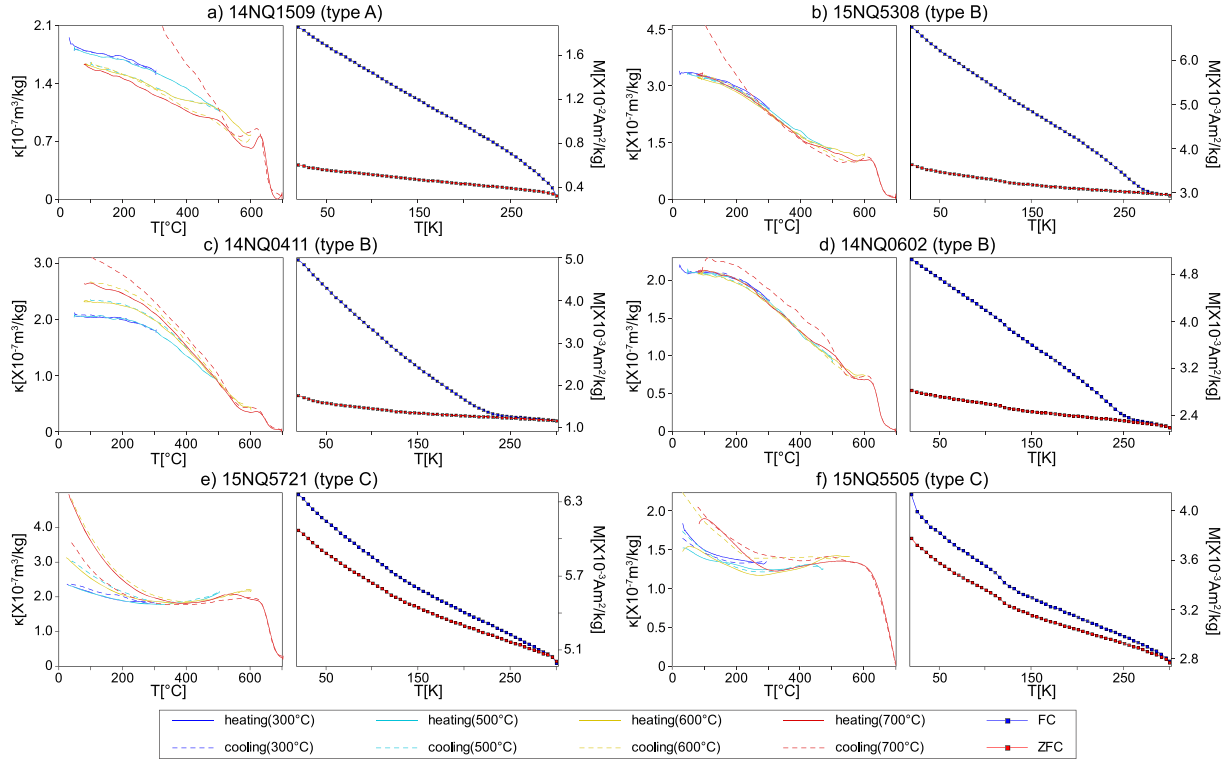

Figure 2. High temperature susceptibility versus temperature (κ-T) curves and field-cooled (FC) and zero-field-cooled (ZFC) curves of representative samples.

temperature spectrum and grain size distribution of magnetic nanoparticles (Worm & Jackson, 1999). The low-temperature saturation isothermal remanent magnetization (SIRM) warming curves after zero-field cooled (ZFC) and field cooled (FC) treatments for all samples show continuous decay in remanence during warming (Figure 2), further implying a wide distribution of magnetic grain size and a strong superparamagnetic (SP) portion at room temperature. The Verwey transition of magnetite at 120 K is displayed in most samples, whereas the Morin transition of hematite at 250–260 K is likely smeared out by progressive unblocking of SP hematite. Types A and B samples have widely separated FC and ZFC curves (Figures 2a–2d) with a high ratio (>2) of FC versus ZFC remanence (M_{FC}/M_{ZFC}) at 20 K (Figure S4b, Table S4), pointing to the presence of goethite (Guyodo et al., 2003; Liu et al., 2006). In contrast, FC and ZFC curves of Type C samples are not widely separated (Figures 2e and 2f), with M_{FC}/M_{ZFC} at 20 K of ~1 (Figure S4b, Table S4). The low-temperature cycling curves of a room-temperature SIRM for one Type A sample show a steep increase in remanence on cooling and a slight net loss of magnetization when warming up to room temperature (Figure 3a), indicating a high concentration of goethite in these samples in addition to fine-grained hematite (France & Oldfield, 2000). After removing the contribution of soft magnetic carriers by applying an alternating field (AF) demagnetization with a peak field of 200 mT, the room-temperature SIRM cooling and warming curves for this sample are reversible up to 300 K. The warming curves then show a sharp drop in remanence at 300–350 K [lower than Néel temperature of goethite at 393 K, O'reilly, 1984] and continuous loss of remanence up to 400 K with irreversible cooling curves from 400 to 20 K. The other two sample types (A and B) show an irreversible decrease in remanence on cooling to 20 K and a substantial net loss of remanence when warming to room temperature, and weak signals of the Verwey and Morin translations are discernable (Figures 3b and 3c). After AF demagnetization, the warming curves show a gentle decrease in remanence between 350 and 400 K and are irreversible when compared to the cooling curves of 400–20 K. The decrease in remanence between 350 and 400 K for all Types A and B samples possibly represents unblocking of fine-grained hematite instead of goethite. Compared to the Type A sample showing a sharp drop in remanence at 300–350 K on the warming curves after AF demagnetization, the two Types A and B samples without the sharp drop may contain less goethite and/or finer goethite which unblocks together with fine-grained hematite. Type C samples have similar room

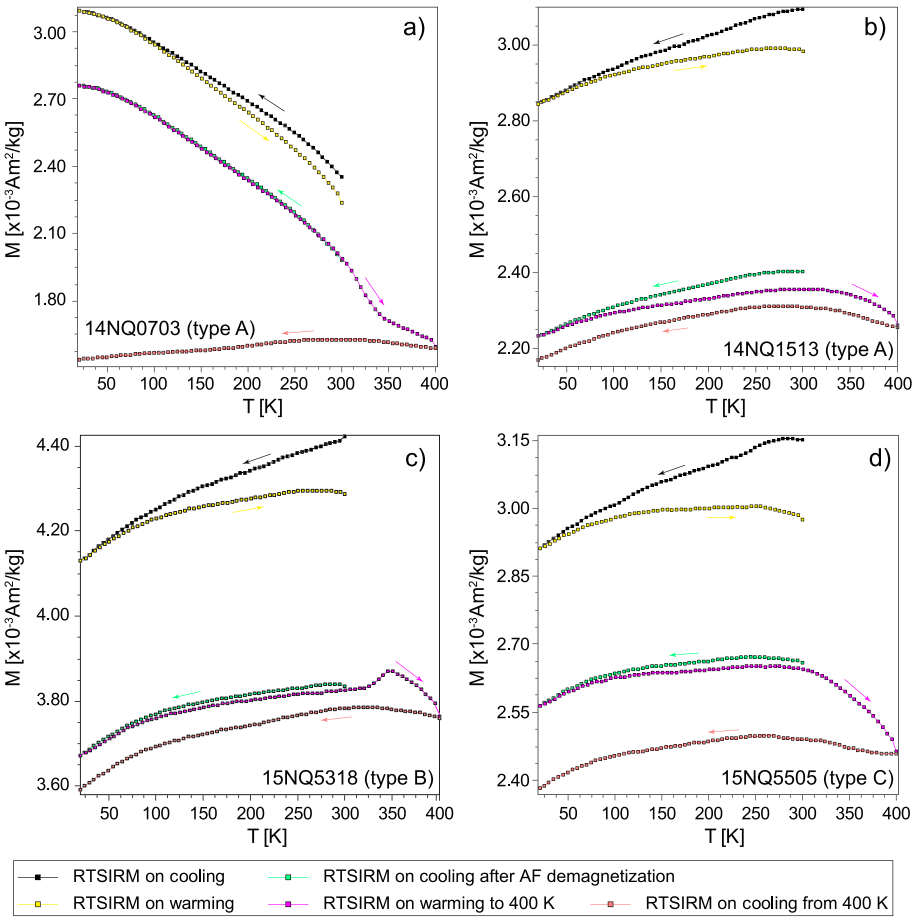

Figure 3. Cycling of the room temperature saturation remanent magnetization for the representative samples. The samples were first given a 2.5 T field and then measured during a cooling (black) and warming (yellow) cycle between 300 and 20 K. Next, the samples were demagnetized by an alternating field with a peak of 200 mT. The remaining remanence is then measured when cooling (green) down to 20 K. Finally, remanence was measured when samples were warmed (purple) and cooled (pink) between 20 and 400 K.

temperature SIRM cycling curves to these Types A and B samples without the sharp drop in remanence both before and after AF demagnetization (Figure 3d). The gradual decrease in remanence above 300 K in the warming curves after AF demagnetization is due to unblocking of fine-grained hematite.

To better discriminate fine-grained hematite and goethite, we then applied Mössbauer spectroscopy (see supporting information for methods). The Mössbauer spectrum at 295 K from one Type A sample is represented by two sextets and three doublets (Figure 4, Table S5). One minor sextet fitted with a hyperfine field distribution with a smaller magnetic hyperfine field (B_{HF}) of 35.35 T has parameters close to those of goethite at room temperature, and the other one, with B_{HF} = 50.98 T, is similar to that of hematite (Dyar et al., 2006). Modeling of the spectra reveals that the 6.4% of the iron resides in room-temperature stable goethite and 42.15% of the iron resides in hematite, with the remainder in paramagnetic or superparamagnetic particles. At 18 K, the Mössbauer spectrum of this sample was also fitted by two sextets, corresponding to goethite (28.67%) and hematite (44.71%) and three doublets (Figure 4a). The Mössbauer spectrum for a Type B sample is fitted by two sextets (one crystalline site and one minor hyperfine field distribution, both representing hematite) and three doublets at 295 K, whereas at 18 K the two fitted sextets are due to goethite (23.81%) and hematite (44.32%) (Figure 4b). For the two Type C samples (Figures 4c and 4d), the Mössbauer spectrum is fitted by two sextets (again both representing hematite) and two doublets at 295 K and one sextet (corresponding to hematite) and two doublets at 18 K. The modeled hematite contribution also slightly increases at 18 K when compared to that at 295 K (Table S5). The fitted B_{HF} values for all samples from the Nangqian red

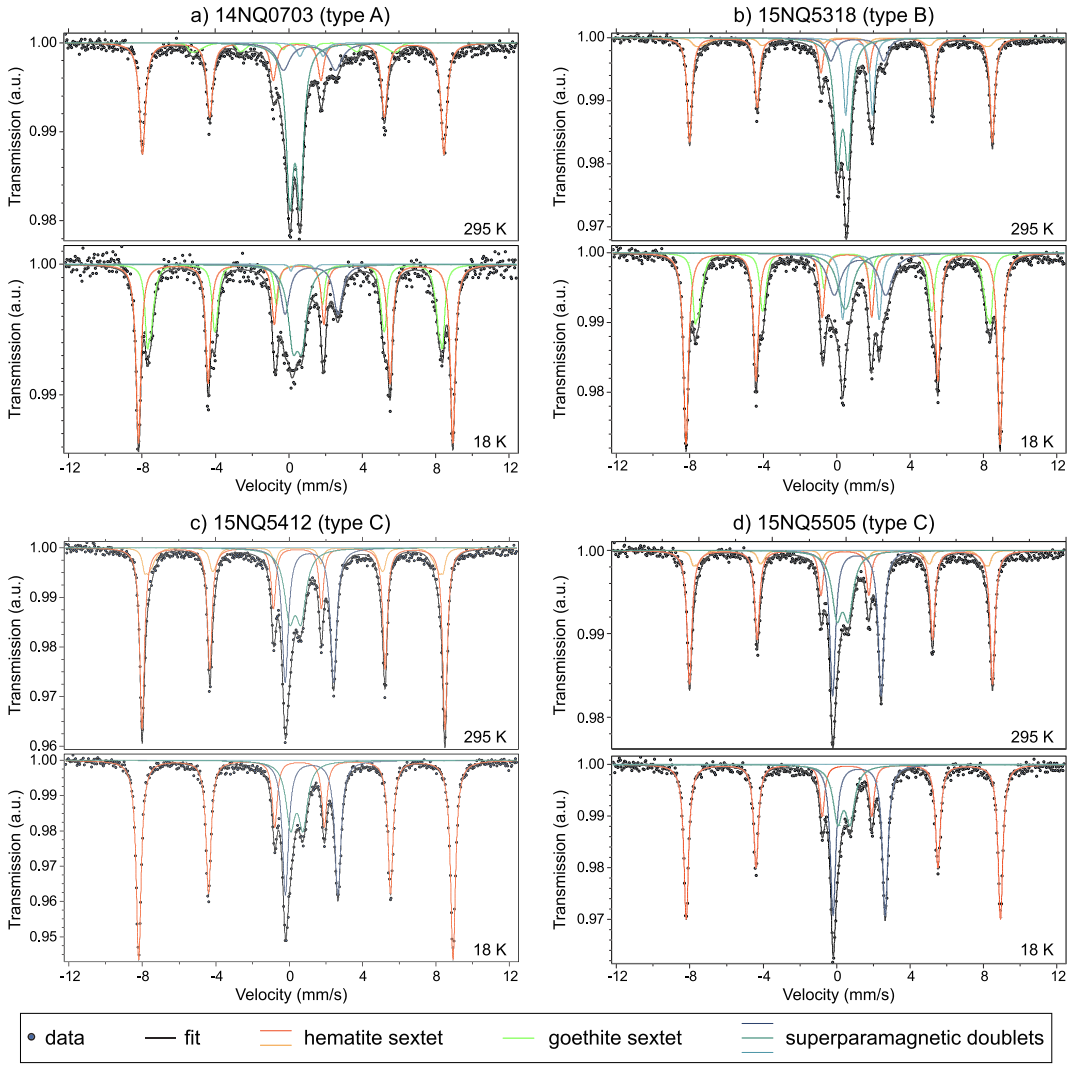

Figure 4. Mössbauer spectrum acquired at 295 and 18 K for powder red bed samples. Dots with the black lines are data and model fits. Red and yellow sextets are the fits diagnostic of hematite; green sextet represents goethite (significant only in Types A and B samples, especially at low temperature). The central peaks comprised superposed doublets dominated by Fe^{3+}.

beds are reduced when compared to stoichiometric goethite and hematite at 295 or 18 K, and this is likely related to structural defects or small particle size of goethite and hematite (Berquó et al., 2007). The significant increase in the modeled goethite contribution and the decrease in the paramagnetic doublets in Types A and B samples at 18 K indicate that most of the goethite grains are (super)paramagnetic at room temperature but are blocked at 18 K. The slight increase in the content of the hematite sextet in all the samples at 18 K (Table S5) is likely associated with ordering of the smallest nanoparticles of hematite (Bødker et al., 2000). Our Mössbauer spectroscopy analyses thus confirm the presence of nanogoethite in Types A and B samples and that Type C samples contain an undetectable amount (<2%) of goethite.

To visually and chemically characterize the differences in magnetic minerals, we further conducted scanning electron microscopy and X-ray spectrometry examinations (see supporting information for methods). In Type C samples, plate-like detrital hematite at length scales of a few microns and minor detrital titanomagnetite with solid-state exsolution features at size of 5–50 μm are the main phase of magnetic minerals (Figures 5a–5e), although very fine needle-shaped hematite is well-presented (Figure 5e). Early diagenetic pyrite is also preserved (Figure 5f). In Types A and B samples, authigenic magnetite pseudomorphic after

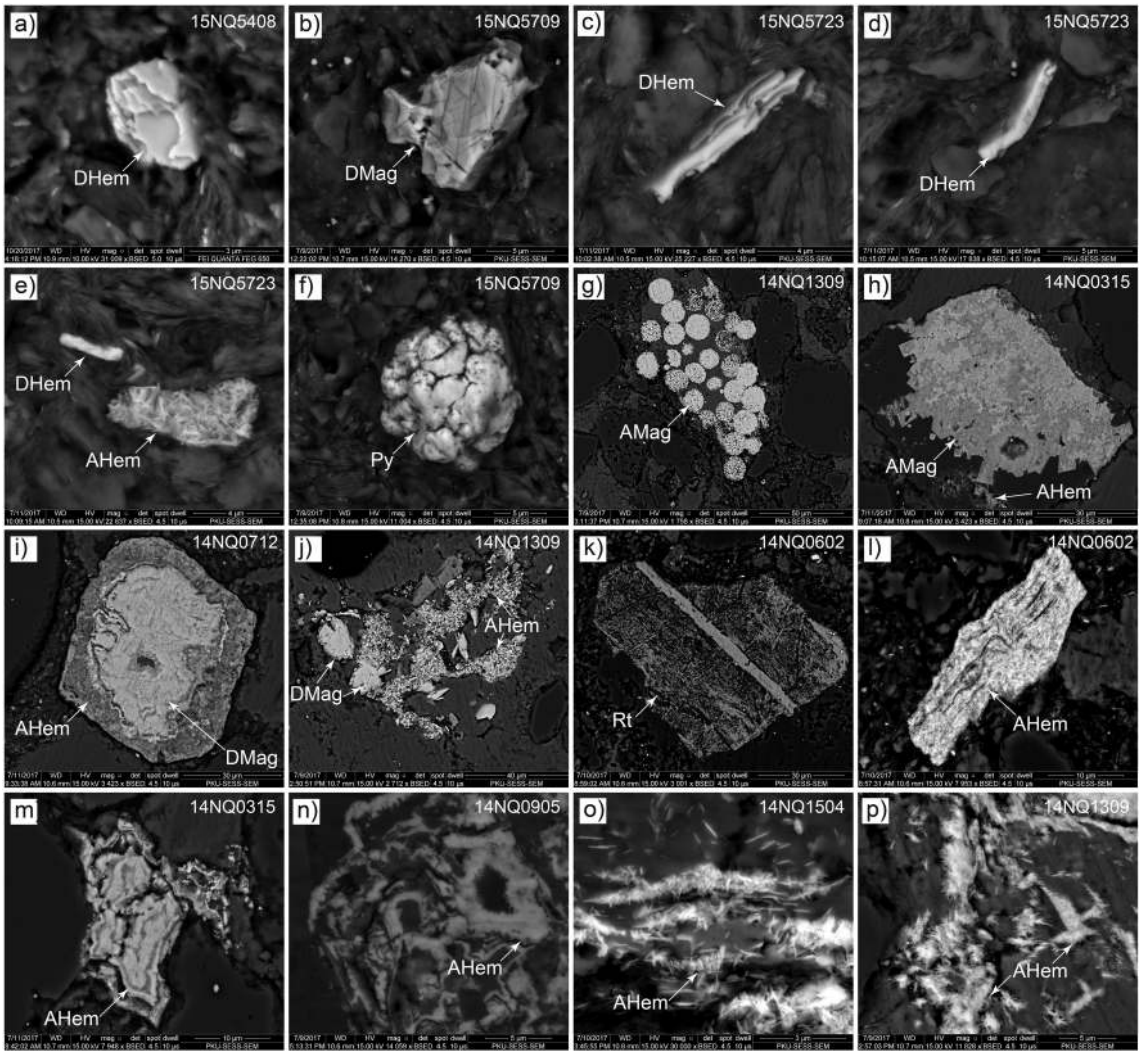

Figure 5. SEM backscattered electron images of samples from the Nangqian red beds (a–f) from Type C samples, (i,o) from Type A samples, and the remainder are from Type B samples. DHem = detrital hematite; AHem = authigenic hematite; DMag = detrital magnetite; AMag = authigenic magnetite; Py = pyrite; Rt = rutile.

framboidal or subeuhedral to euhedral pyrite is observed (Figures 5g and 5h). Detrital titanomagnetite and hematite have been extensively altered with iron leached and deposited as authigenic hematite (Figures 5i–5p). Omnipresent authigenic hematite replaces the preexisting detrital titanomagnetite and hematite, shows growth zoning, and is mostly needle-shaped grains with length <1 μm and width <0.1 μm.

3. Discussion

Detrital and authigenic hematite are the principal magnetic carriers in the Nangqian red beds; the minor magnetic phase of magnetite also has both detrital and authigenic origin. According to the hematite grain volume and unblocking temperature relationship (Swanson-Hysell et al., 2011), the diameter of hematite grains can be estimated. Type A samples have the widest unblocking temperature spectrum up to the Néel temperature, indicating that hematite grain size varies from the SP-stable single domain threshold [<tens nm, Swanson-Hysell et al., 2019] up to >500 nm. The ITC of Type B samples (<650 °C) is mostly carried by hematite grains with diameters of <400 nm, whereas the HTC (>650 °C) is retained in hematite with diameter of >400 nm. Hematite grains carrying the ITC of Type C samples (<300–600 °C) are <200 nm in diameter, and those carrying the HTC are >200 nm. The DRM carried by detrital magnetite is thus

completely swamped in secondary remanence carried by authigenic magnetite and hematite in Types A and B samples.

Considering the limited concentration of authigenic magnetite in the Nangqian red beds (Figure 5), low temperature properties of susceptibility and remanence (Figures 2 and 3) indicate that nanohematite (<tens nm) is abundant in these rocks. Besides, Mössbauer spectra reveal that only small amounts of thermally stable goethite are present in Types A and B samples at room temperature, but at 18 K > 20% of the absorption is due to iron residing in goethite in these samples (Figures 4a and 4b). This value at 18 K is a conservative estimation, because finer goethite may still be unblocked at such temperature, contributing to the central doublets.

Circulation of externally derived magmatic or basinal fluid is not observed in the field and our petrographic examinations (Figure 5). Instead, the thermal anomaly induced by magmatism is probably the controlling factor for the remagnetization, although other factors (e.g., lithology) may also have an effect. This is further supported by the observations that the completely remagnetized Type A samples are adjacent or close to the magmatic bodies, whereas Type C samples retaining primary remanence are relatively far away (Figure 1a). Low-temperature thermochronology studies show that detrital zircon (U-Th)/He [closure temperature: 170–190 °C, Reiners et al., 2004] ages of the red beds are not reset (personal communication with Dr. Lin Li), but apatite (U-Th-Sm)/He [closure temperature: 60–80 °C, Farley, 2000] ages of the magmatic rocks are reset [20–15 Ma, Dai et al., 2013]. Reset clumped isotope of carbonate interbedded with the Nangqian red beds yield $T(\Delta_{47})$ values of 45–76.5 °C (Li et al., 2018), which should be between the surface and peak temperatures according to the modeled clumped isotope resetting process (Stolper & Eiler, 2015). Therefore, it is likely that the Nangqian red beds were inhomogeneously heated up to 100–170 °C during the magmatism, followed by a later homogeneous burial heating to >60 °C. During the diagenesis at 38–37 Ma, alteration of detrital hematite, magnetite, other Fe-bearing phases, and early diagenetic pyrite leached iron, forming ferrihydrite. In the crystallization of hematite and goethite from precursor ferrihydrite, their ratio strongly depends on temperature (e.g., Das et al., 2011; Jiang et al., 2016). Type A samples closer to the magmatic bodies suffered from the most intense heating: Detrital magnetic particles were almost completely altered, and authigenic hematite grew to >500 nm with unblocking temperature up to 680 °C (Figure 1b). Goethite in some Type A samples grew to large grains with unblocking temperatures of 27–77 °C (Figure 3a), and the absolute abundance of goethite is high (Figure 4a). Type B samples suffered from intermediate heating: Large detrital magnetic particles survived alteration, and some authigenic hematite grew to moderate sizes (>400 nm) with high unblocking temperatures (>650 °C); the DRM carried by the large detrital hematite was thus contaminated or overprinted (Figures 1c and 1d). Goethite in these samples is finer and less abundant (Figures 3c and 4b, Table S5). Type C samples were the least heated and altered; small detrital magnetic particles were altered, authigenic hematite never grew above 200 nm, and DRM carried by detrital hematite can be isolated at >600 °C (Figures 1e and 1f). Goethite is undetectable in these samples (Figures 3d and 4d, Table S5), although it should have been formed simultaneously with dominant hematite (Das et al., 2011). The reason might be that the crystallized goethite grains were the finest, thermodynamically unstable, and dehydrated to hematite during subsequent burial heating (Berner, 1969; Till et al., 2015; Weibel & Grobety, 1999). A difference in redox conditions, shown by alteration of early diagenetic pyrite to authigenic magnetite in Types A and B samples and the preservation of pyrite in Type C samples (Figures 5f–5h), may also have contributed to the remagnetization, similar to the remagnetization of the Tethyan limestones (Huang, Lippert, Dekkers, et al., 2017; Huang, Lippert, Zhang, et al., 2017; Huang et al., 2019).

Consistent with the argument that concave (convex) shape of thermal decay curves potentially indicates CRM (DRM) (Jiang et al., 2015), thermal decay curves of different types of the Nangqian red beds samples are distinct (Figure S6). We find, however, that convex thermal decay curves of some Type A samples and the high temperature portion of Type B samples cannot be correctly interpreted. High temperature κ-T curves of Types A and B samples have a small hump above 550 °C before a sharp but insignificant drop near the Néel temperature of hematite, whereas κ-T curves of Type C samples show a big hump near 300 °C followed by a sharp and significant drop near the Néel temperature (Figure 2). More importantly, we find that Types A and B samples contain a large amount of nanogoethite, characterized by widely separated FC and ZFC curves (Figure 2) and the appearance of a significant goethite sextet in the Mössbauer spectrum (Figures 4a and 4b) at low temperature. In contrast, little goethite is detected in Type C samples (Figures 2 and 4). Therefore, in addition to the shape of thermal decay curves of the remanence, and high

temperature κ-T behavior, the presence of nanogoethite is potentially a sensitive indicator for remagnetization in red beds.

Trace amounts of goethite have been detected by thermal demagnetization of the composite IRMs in remagnetized Jurassic to Cretaceous red beds (Tsuchiyama et al., 2016; Yamashita et al., 2011). We realize, however, that most goethite grains in remagnetized red beds are possibly nanoscaled and can be detected by low-temperature experiments at best. To verify the universal existence of goethite in remagnetized red beds, low-temperature tests are required to systematically apply to more profiles in the future. We emphasize here that goethite detected in this research is not related to recent weathering or groundwater flowing. Fresh samples were commonly taken after deep digging during the fieldwork, and goethite could have been detected in all types of samples if this was the case.

4. Conclusions

Our study supports the proposition that CRM and DRM can be distinguished by difference in unblocking temperatures of authigenic and detrital hematite. More importantly, we find that authigenic hematite can grow to relatively large sizes, overlapping with those of detrital hematite, and CRM can thus completely replace or contaminate the DRM. Preservation of DRM in red beds depends on separation of unblocking temperatures and grain sizes between authigenic and detrital hematite, which is controlled by postdepositional temperatures in our case. Heating induced by burial or magmatism is possibly one of the main reasons for remagnetization of red beds, especially for those in tectonically active orogenic belts. We emphasize that directional change at high unblocking temperatures is not enough to discriminate DRM from CRM in red beds. Combined rock magnetic tests, Mössbauer spectroscopy analyses, and petrographic examinations should be carried out to evaluate the potential preservation of DRM in red beds. The presence of significant amounts of nanogoethite potentially indicates remagnetization in red beds.

Acknowledgments

Data to support this article are available in supporting information Tables S1–S6, which are also deposited in Zenodo (34e50cc1f9cbe4dd35c2a62c35ee91e6). W.H. was supported by three visiting research fellowships from the Institute for Rock Magnetism (IRM) at the University of Minnesota, which is funded by the Instruments and Facilities program of NSF. We thank Dr. Dario Bilardello at the IRM, and Dr. Peter C. Lippert at Utah Pmag Center for laboratory assistance. Dr. Pierrick Roperch and Dr. Guillaume Dupont-Nivet are especially appreciated for sharing the thermal demagnetization data and discussing. We are also grateful to Dr. Swanson-Hysell and two anonymous reviewers for their constructive comments, which have greatly helped improve the original manuscript.

References

Berner, R. A. (1969). Goethite stability and the origin of red beds. *Geochimica et Cosmochimica Acta*, *33*(2), 267–273. https://doi.org/10.1016/0016-7037(69)90143-4

Berquó, T. S., Imbernon, R. A. L., Blot, A., Franco, D. R., Toledo, M. C. M. D., & Partiti, C. S. D. M. (2007). Low temperature magnetism and Mössbauer spectroscopy study from natural goethite. *Physics and Chemistry of Minerals*, *34*(5), 287–294. https://doi.org/10.1007/s00269-007-0147-9

Bødker, F., Hansen, M. F., Koch, C. B., Lefmann, K., & Mørup, S. (2000). Magnetic properties of hematite nanoparticles. *Physical Review B*, *61*(10), 6826–6838. https://doi.org/10.1103/PhysRevB.61.6826

Dai, J., Wang, C., Hourigan, J., & Santosh, M. (2013). Insights into the early Tibetan Plateau from (U–Th)/He thermochronology. *Journal of the Geological Society*, *170*(6), 917–927. https://doi.org/10.1144/jgs2012-076

Das, S., Hendry, M. J., & Essilfie-Dughan, J. (2011). Transformation of two-line ferrihydrite to goethite and hematite as a function of pH and temperature. *Environmental Science & Technology*, *45*(1), 268–275. https://doi.org/10.1021/es101903y

Deng, C., Liu, Q., Wang, W., & Liu, C. (2007). Chemical overprint on the natural remanent magnetization of a subtropical red soil sequence in the Bose Basin, southern China. *Geophysical Research Letters*, *34*, L22308. https://doi.org/10.21029/22007GL031400

Dupont-Nivet, G., Krijgsman, W., Langereis, C. G., Abels, H. A., Dai, S., & Fang, X. M. (2007). Tibetan plateau aridification linked to global cooling at the Eocene-Oligocene transition. *Nature*, *445*(7128), 635–638. https://doi.org/10.1038/nature05516

Dyar, M. D., Agresti, D. G., Schaefer, M. W., Grant, C. A., & Sklute, E. C. (2006). Mössbauer spectroscopy of earth and planetary materials. *Annual Review of Earth and Planetary Sciences*, *34*(1), 83–125. https://doi.org/10.1146/annurev.earth.34.031405.125049

Farley, K. (2000). Helium diffusion from apatite: General behavior as illustrated by Durango fluorapatite. *Journal of Geophysical Research*, *105*(B2), 2903–2914. https://doi.org/10.1029/1999JB900348

France, D., & Oldfield, F. (2000). Identifying goethite and hematite from rock magnetic measurements of soils and sediments. *Journal of Geophysical Research*, *105*(B2), 2781–2795. https://doi.org/10.1029/1999JB900304

Guyodo, Y., Mostrom, A., Penn, R. L., & Banerjee, S. K. (2003). From nanodots to nanorods: Oriented aggregation and magnetic evolution of nanocrystalline goethite. *Geophysical Research Letters*, *30*(10), 1512. https://doi.org/10.1029/2003GL017021

Horton, B. K., Yin, A., Spurlin, M. S., Zhou, J., & Wang, J. (2002). Paleocene-Eocene syncontractional sedimentation in narrow, lacustrine-dominated basins of east-central Tibet. *Geological Society of America Bulletin*, *114*(7), 771–786. https://doi.org/10.1130/0016-7606(2002)114<0771:PESSIN>2.0.CO;2

Huang, W., Jackson, M. J., Dekkers, M. J., Zhang, Y., Zhang, B., Guo, Z., & Dupont-Nivet, G. (2019). Challenges in isolating primary remanent magnetization from Tethyan carbonate rocks on the Tibetan Plateau: Insight from remagnetized Upper Triassic limestones in the eastern Qiangtang block. *Earth and Planetary Science Letters*, *523*, 115695. https://doi.org/10.1016/j.epsl.2019.06.035

Huang, W., Lippert, P. C., Dekkers, M. J., Jackson, M. J., Zhang, Y., Li, J., et al. (2017). Remagnetization of the Paleogene Tibetan Himalayan carbonate rocks in the Gamba area: Implications for reconstructing the lower plate in the India-Asia collision. *Journal of Geophysical Research: Solid Earth*, *122*, 808–825. https://doi.org/10.1002/2016JB013662

Huang, W., Lippert, P. C., Zhang, Y., Jackson, M. J., Dekkers, M. J., Li, J., et al. (2017). Remagnetization of carbonate rocks in southern Tibet: Perspectives from rock magnetic and petrographic investigations. *Journal of Geophysical Research: Solid Earth*, *122*, 2434–2456. https://doi.org/10.1002/2017JB013987

Jiang, Z., Liu, Q., Dekkers, M. J., Barrón, V., Torrent, J., & Roberts, A. P. (2016). Control of Earth-like magnetic fields on the transformation of ferrihydrite to hematite and goethite. *Scientific Reports*, *6*, 30395. https://doi.org/10.1038/srep30395

Jiang, Z., Liu, Q., Dekkers, M. J., Tauxe, L., Qin, H., Barrón, V., & Torrent, J. (2015). Acquisition of chemical remanent magnetization during experimental ferrihydrite–hematite conversion in Earth-like magnetic field—Implications for paleomagnetic studies of red beds. *Earth and Planetary Science Letters*, *428*, 1–10. https://doi.org/10.1016/j.epsl.2015.07.024

Jiang, Z., Liu, Q., Dekkers, M. J., Zhao, X., Roberts, A. P., Yang, Z., et al. (2017). Remagnetization mechanisms in Triassic red beds from South China. *Earth and Planetary Science Letters*, *479*, 219–230. https://doi.org/10.1016/j.epsl.2017.09.019

Kruiver, P. P., Dekkers, M. J., & Langereis, C. G. (2000). Secular variation in Permian red beds from Dôme de Barrot, SE France. *Earth and Planetary Science Letters*, *179*(1), 205–217. https://doi.org/10.1016/S0012-821X(00)00104-7

Li, L., Fan, M., Davila, N., Jesmok, G., Mitsunaga, B., Tripati, A., & Orme, D. (2018). Carbonate stable and clumped isotopic evidence for late Eocene moderate to high elevation of the east-central Tibetan Plateau and its geodynamic implications. *Geological Society of America Bulletin*, *131*, 831–844. https://doi.org/10.1130/B32060.1

Li, S., Advokaat, E. L., van Hinsbergen, D. J., Koymans, M., Deng, C., & Zhu, R. (2017). Paleomagnetic constraints on the Mesozoic-Cenozoic paleolatitudinal and rotational history of Indochina and South China: Review and updated kinematic reconstruction. *Earth-Science Reviews*, *171*, 58–77. https://doi.org/10.1016/j.earscirev.2017.05.007

Liu, Q., Yu, Y., Torrent, J., Roberts, A. P., Pan, Y., & Zhu, R. (2006). Characteristic low-temperature magnetic properties of aluminous goethite [α-(Fe, Al) OOH] explained. *Journal of Geophysical Research*, *111*, B12S34. https://doi.org/10.1029/2006JB004560

O'reilly, W. (1984). *Rock and mineral magnetism*. New York, NY: Chapman & Hall.

Özdemir, Ö., & Dunlop, D. J. (2014). Hysteresis and coercivity of hematite. *Journal of Geophysical Research: Solid Earth*, *119*, 2582–2594. https://doi.org/10.1002/2013JB010739

Reiners, P. W., Spell, T. L., Nicolescu, S., & Zanetti, K. A. (2004). Zircon (U-Th)/He thermochronometry: He diffusion and comparisons with $^{40}Ar/^{39}Ar$ dating. *Geochimica et Cosmochimica Acta*, *68*(8), 1857–1887. https://doi.org/10.1016/j.gca.2003.10.021

Roperch, P., Dupont-Nivet, G., Guillot, S., Goussin, F., Huang, W., Replumaz, A., et al. (2017). Paleomagnetic constraints on early collisional deformation along the eastern margin of the Qiangtang terrane (Tibetan plateau) at 50 and 37 Ma, paper presented at EGU General Assembly Conference Abstracts.

Spurlin, M. S., Yin, A., Horton, B. K., Zhou, J., & Wang, J. (2005). Structural evolution of the Yushu-Nangqian region and its relationship to syncollisional igneous activity, east-central Tibet. *Geological Society of America Bulletin*, *117*(9), 1293–1317. https://doi.org/10.1130/B25572.1

Stearns, C., & Van der Voo, R. (1987). A paleomagnetic reinvestigation of the Upper Devonian Perry Formation: Evidence for Late Paleozoic remagnetization. *Earth and Planetary Science Letters*, *86*(1), 27–38. https://doi.org/10.1016/0012-821X(87)90185-3

Stolper, D. A., & Eiler, J. M. (2015). The kinetics of solid-state isotope-exchange reactions for clumped isotopes: A study of inorganic calcites and apatites from natural and experimental samples. *American Journal of Science*, *315*(5), 363–411. https://doi.org/10.2475/05.2015.01

Swanson-Hysell, N. L., Fairchild, L. M., & Slotznick, S. P. (2019). Primary and secondary red bed magnetization constrained by fluvial intraclasts. *Journal of Geophysical Research: Solid Earth*, *124*, 4276–4289. https://doi.org/10.1029/2018jb017067

Swanson-Hysell, N. L., Feinberg, J. M., Berquó, T. S., & Maloof, A. C. (2011). Self-reversed magnetization held by martite in basalt flows from the 1.1-billion-year-old Keweenawan rift, Canada. *Earth and Planetary Science Letters*, *305*(1-2), 171–184. https://doi.org/10.1016/j.epsl.2011.02.053

Tauxe, L., & Kent, D. V. (2004). A simplified statistical model for the geomagnetic field and the detection of shallow bias in paleomagnetic inclinations: Was the ancient magnetic field dipolar? In *Timescales of the Paleomagnetic field*, *Geophysical Monograph Series* (Vol. 145, pp. 101–115). Washington, DC: American Geophysical Union. https://doi.org/10.1029/1145GM1008

Tauxe, L., Mullender, T., & Pick, T. (1996). Potbellies, wasp-waists, and superparamagnetism in magnetic hysteresis. *Journal of Geophysical Research*, *101*(B1), 571–583. https://doi.org/10.1029/1095JB03041

Till, J., Guyodo, Y., Lagroix, F., Morin, G., & Ona-Nguema, G. (2015). Goethite as a potential source of magnetic nanoparticles in sediments. *Geology*, *43*(1), 75–78. https://doi.org/10.1130/G36186.1

Tong, Y., Yang, Z., Mao, C., Pei, J., Pu, Z., & Xu, Y. (2017). Paleomagnetism of Eocene red-beds in the eastern part of the Qiangtang Terrane and its implications for uplift and southward crustal extrusion in the southeastern edge of the Tibetan Plateau. *Earth and Planetary Science Letters*, *475*, 1–14. https://doi.org/10.1016/j.epsl.2017.07.026

Tsuchiyama, Y., Zaman, H., Sotham, S., Samuth, Y., Sato, E., Ahn, H.-S., et al. (2016). Paleomagnetism of Late Jurassic to Early Cretaceous red beds from the Cardamom Mountains, southwestern Cambodia: Tectonic deformation of the Indochina Peninsula. *Earth and Planetary Science Letters*, *434*, 274–288. https://doi.org/10.1016/j.epsl.2015.11.045

Weibel, R., & Grobety, B. (1999). Pseudomorphous transformation of goethite needles into hematite in sediments of the Triassic Skagerrak Formation, Denmark. *Clay Minerals*, *34*(4), 657–660. https://doi.org/10.1180/000985599546415

Worm, H. U., & Jackson, M. (1999). The superparamagnetism of Yucca Mountain tuff. *Journal of Geophysical Research*, *104*(B11), 25,415–25,425. https://doi.org/10.1029/21999JB900285

Xian, H., Zhang, S., Li, H., Xiao, Q., Chang, L., Yang, T., & Wu, H. (2019). How did South China connect to and separate from Gondwana? New Paleomagnetic Constraints from the Middle Devonian Red Beds in South China. *Geophysical Research Letters*, *46*, 7371–7378. https://doi.org/10.1029/2019GL083123

Yamashita, I., Surinkum, A., Wada, Y., Fujihara, M., Yokoyama, M., Zaman, H., & Otofuji, Y.-i. (2011). Paleomagnetism of the Middle–Late Jurassic to Cretaceous red beds from the Peninsular Thailand: Implications for collision tectonics. *Journal of Asian Earth Sciences*, *40*(3), 784–796. https://doi.org/10.1016/j.jseaes.2010.11.001

Zhang, Y., Huang, W., Huang, B., van Hinsbergen, D. J. J., Yang, T., Dupont-Nivet, G., & Guo, Z. (2018). 53-43 Ma deformation of the Eastern Tibet revealed by three stages of tectonic rotation in the Gongjue basin. *Journal of Geophysical Research: Solid Earth*, *123*, 3320–3338. https://doi.org/10.1002/2018JB015443